metals

MDPI

Article

Effect of Rotary Swaging on Microstructure and Properties of Cr-Ni-Ti Austenitic Stainless Steel

Olga Rybalchenko [1], Vladimir Torganchuk [2], Georgy Rybalchenko [3], Natalia Martynenko [1], Elena Lukyanova [1], Alexey Tokar [1,4], Dmitry Prosvirnin [1], Vladimir Yusupov [1] and Sergey Dobatkin [1,4,*]

[1] A.A. Baikov Institute of Metallurgy and Materials Science of the Russian Academy of Science, Leninskiy Prospect, 49, 119334 Moscow, Russia; orybalchenko@imet.ac.ru (O.R.); nmartynenko@imet.ac.ru (N.M.); elukyanova@imet.ac.ru (E.L.); tokar.aa@misis.ru (A.T.); vyusupov@imet.ac.ru (V.Y.)
[2] Laboratory of Mechanical Properties of Nanostructured Materials and Superalloys, Belgorod State University, Pobeda St., 85, 308015 Belgorod, Russia; torganv@mail.ru
[3] P.N. Lebedev Physical Institute of the Russian Academy of Science, Leninsky Prospect, 53, 119991 Moscow, Russia; rybalchenkogv@lebedev.ru
[4] Department of Physical Materials Science, National University of Science and Technology "MISIS", Leninsky Prospect, 4, 119049 Moscow, Russia
* Correspondence: sdobatkin@imet.ac.ru

Abstract: In this study, Cr-Ni-Ti austenitic stainless steel was subjected to rotary swaging in various modes, followed by annealing. The effect of processing conditions on the resulting microstructure and, therefore, on the mechanical properties under static and cyclic loading was studied. After RS the formation of an ultrafine-grained predominantly twinned structure, with structural elements sized between 100–250 nm in Cr-Ni-Ti stainless steel, was observed. The stepwise temperature reduction during rotary swaging allows the manipulation of the microstructure transformations, which eventually leads to the desired properties of the steel. As a result, the ultimate tensile strength increased from 610 MPa to 1304 MPa when the elongation decreased from 40% to 10.5%, and the fatigue limit increased from 425 MPa to 700 MPa. The Cr-Ni-Ti steel is strengthened through the formation of an ultrafine-grained structure, twinning in austenite, and martensitic transformation. Subsequent annealing at a temperature 475 °C triggers the active precipitation of nanosized TiC carbides in the deformed steel. On one hand, the presence of these carbides increases the tensile strength up to 1938 Mpa, while on the other hand, slows down crack propagation with a slight decrease in ductility (ε = 8%) of the deformed sample. At the same time, dispersion hardening does not affect the fatigue limit of steel.

Keywords: Cr-Ni-Ti stainless steel; rotary swaging; ultrafine grained microstructure; strain-induced martensite; twinning; mechanical properties; carbides

Citation: Rybalchenko, O.; Torganchuk, V.; Rybalchenko, G.; Martynenko, N.; Lukyanova, E.; Tokar, A.; Prosvirnin, D.; Yusupov, V.; Dobatkin, S. Effect of Rotary Swaging on Microstructure and Properties of Cr-Ni-Ti Austenitic Stainless Steel. *Metals* **2023**, *13*, 1760. https://doi.org/10.3390/met13101760

Academic Editor: Giovanni Meneghetti

Received: 11 September 2023
Revised: 9 October 2023
Accepted: 13 October 2023
Published: 17 October 2023

1. Introduction

Cr-Ni austenitic stainless steels are widely used in various industries. However, one of their limitations is their low yield strength, which can be significantly improved by refining the steel structure to an ultrafine-grained (UFG) state through the application of severe plastic deformation (SPD) methods. These techniques allow to refine the grain of the steel effectively. This usually enhances mechanical and performance properties. The possibility of obtaining an ultrafine-grained (UFG) structure in austenitic corrosion-resistant steels is well known through various SPD methods such as equal channel angular pressing (ECAP) [1–8], high-pressure torsion (HPT) [9–14], accumulative roll bonding [15–17], and multidirectional forging [18–20]. These techniques result in improved mechanical and performance characteristics of the steels, making them more suitable for a wide range of applications. Unfortunately, the methods of severe plastic deformation remain challenging for implementation in industrial production settings and can result in high production costs.

Therefore, the development of deformation modes under industrial conditions for achieving an ultrafine-grained structure becomes of paramount importance. It is crucial to explore and optimize deformation techniques that can effectively refine the structure to an ultrafine-grained (UFG) state, while being feasible and cost-effective for industrial-scale production.

Indeed, there are examples of the industrial obtaining of ultrafine-grained austenitic stainless steels through cold rolling followed by short-duration annealing at temperatures above 650 °C [21–24]. Another method of industrial deformation used, for example, in the automotive industry, is rotary swaging (RS). In addition to structure refinement, this method allows pipes, rods and wires to be formed into their final shape with minimal subsequent processing. RS is a cost-effective and efficient technique that can be employed to achieve desired shapes and dimensions in the production of various components. During the RS process, deformation is carried out in small steps, which create a more homogeneous microstructure throughout the workpiece. This stepwise deformation makes RS more efficient for processing compared to continuous deformation methods. The prospects of using RS were shown on various metals and alloys, for example, titanium alloys [25,26], carbon steels [27–29], copper alloys [30,31], zirconium and its alloys [32,33], zinc alloys [34], etc. The influence of RS on the structure and mechanical properties of metastable austenitic stainless steels is still not well studied, but the results obtained by this study are encouraging [35,36]. However, it is evident that by employing different deformation regimes, a wide range of properties for such steels can be achieved. This study did not aim to scale the technology or obtain the final product with the desired properties. The goal was to demonstrate the possibility of optimizing material properties by adding a suitable thermomechanical processing regime to the process of giving the final shape to the product. The exploration of various deformation parameters and conditions can provide the opportunity to tailor the properties of metastable austenitic stainless steels according to specific application requirements.

In this study, RS was employed to form an UFG structure in meta-stable Cr-Ni-Ti austenitic stainless steel. The Cr-Ni-Ti stainless steel is promising for obtaining UFG structure due to its high initial ductility and the ability to additionally control the phase state through martensitic $\gamma \rightarrow \alpha'$ transformation during plastic deformation. When choosing the deformation modes for obtaining the desired microstructure and mechanical properties of steel, it is important to take into account the influence of many factors, such as Ms (martensite start) and Mf (martensite finish) temperature, grain size, etc. This understanding is critical in designing and controlling the deformation process to achieve desired material properties. For example, it was reported in [12] about obtaining a completely austenitic structure in the same Cr-Ni-Ti stainless steel by using a stepwise mode with a decrease in the HPT temperature (450 °C → 300 °C → 20 °C). The formation of a fully austenite state was explained by decreasing the temperature of martensitic transformation due to the reduction of the grain size. Such a decrease in temperature of martensitic transformation by reducing the grain size was predicted theoretically [37] and demonstrated experimentally [38–41]. Therefore, the purpose of this study is to show the feasibility of using a stepwise RS for the production of bulk semi-finished products from stainless steel with UFG microstructure in various phase states with improved mechanical properties.

2. Materials and Methods

The chemical composition of the Cr-Ni-Ti stainless steel is provided in Table 1. For the initial condition, the material was austenitized at a temperature of 1050 °C for a duration of 1 h, followed by water quenching. This heat treatment process aims to transform the steel into the desired austenitic phase and stabilize its microstructure.

Table 1. Chemical composition of the Cr-Ni-Ti stainless steel.

Elements	C	Cr	Ni	Cu	Ti	Si	Mn	S, P	Fe
Amount (wt.%)	0.07	17.3	9.2	0.2	0.7	0.6	1.4	0.003	balance

Rotary swaging was carried out on a rotary swaging machine RKM 2129.02 (UZM, Sverdlovsk, USSR) (maximum force 8 kN) at a frequency of 1920 min^{-1} and a striker travel of 3 mm using stainless steels billets with 19.6 mm in diameter and 90 mm in length (Figure 1). One revolution of the workpiece around its axis was achieved after eight strikes of the striker. The velocity of linear displacement for the rods ranged from 2 to 4 m/min, while the velocity of the stroke was 0.5–1 m/s. The strain rate ranged from 33 to 200 s^{-1}, with an increase observed as the diameter of the rods decreased. The rod diameter was gradually decreased by 1 mm on each pass of the strikers. At each deformation temperature of the stepwise modes, the rod passed through the strikers 6–7 times. The rods were preheated at a specified temperature for 45 min prior to deformation. When changing the strikers, the rods were heated at the same temperature for 15 min. The tooling utilized in the rotary swaging machine remained at an ambient temperature throughout the swaging process. The final diameter of the rods after RS with total drawing (μ) of 10 was about 6 mm. For these modes, the cumulative strain amounted to ε = 2.36.

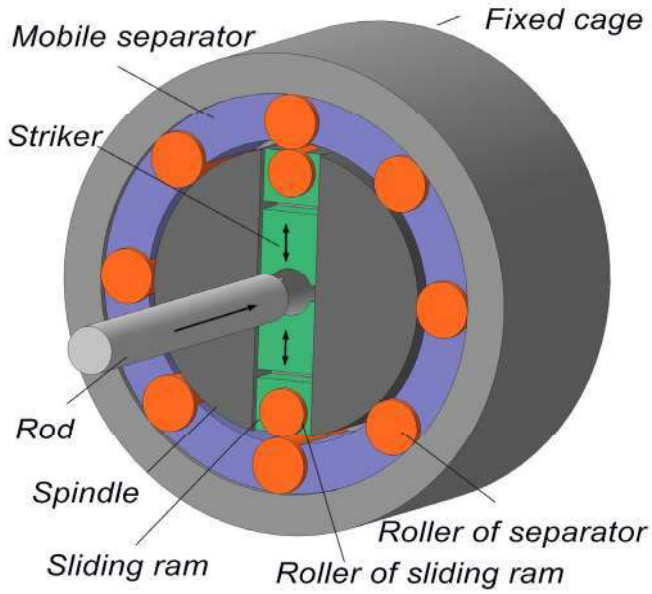

Figure 1. Schematic of the rotary swaging (μ = A_0/A_f, where A_0 and A_f are the initial and the final cross-sectional area of the billets, respectively).

The samples were deformed using the RS method under isothermal conditions at a temperature of 450 °C (RS 450 °C), with a total drawing (μ) of 3 and 10. Additionally, the RS process was performed using two stepwise deformation temperature reduction regimes: from 450 °C to 200 °C (RS 450 → 200 °C) and from 450 °C to 20 °C (RS 450 → 20 °C), with a simultaneous increase in the total drawing (μ) from 3 to 10. The selection of a temperature for the first stage of the RS process, which is above the strain-induced martensite formation temperature, was aimed to obtain a fully austenitic structure in the Cr-Ni-Ti stainless steel after RS with a total drawing (μ) of 3. Subsequent refinements in the structure would enable to suppress the martensitic transformation during further deformation of the steel at a lower temperature of 200 °C.

To determine the mechanical properties, uniaxial tensile tests were performed at room temperature. The tensile tests were conducted using an INSTRON 3380 machine (Instron, Norwood, MA, USA) with a load capacity of 100 kN at a cross-head speed of 1.5 mm/min. Specimens for tensile test were prepared along the swaging direction with samples measuring 3 mm in diameter and 15 mm in length within the working area (Figure 2a). Measurements of microhardness were performed using the 402 MVD Wolpert Wilson instrument by applying a load of 1 N at an indentation time of 10 s.

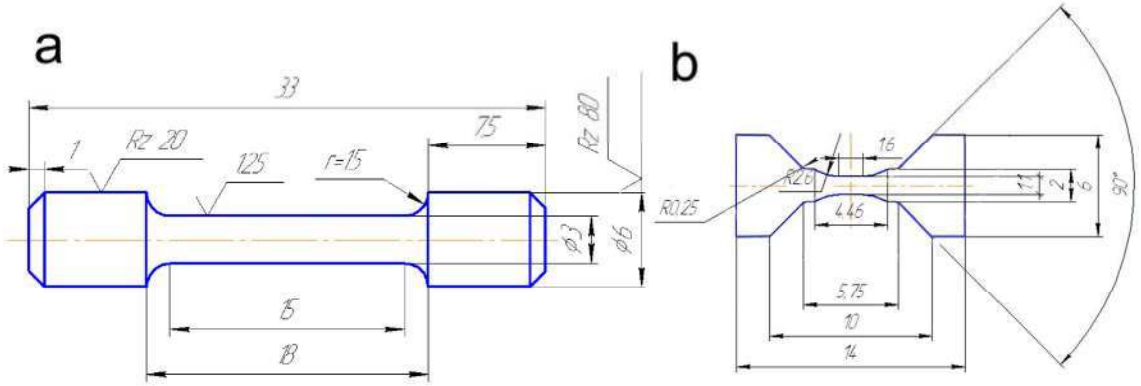

Figure 2. Schematic representation showing testing samples for tensile tests (**a**) and fatigue tests (**b**).

The microstructure analysis was investigated using an Olympus PME 3 optical microscope and a JEM-2100 transmission electron microscope (JEOL; Tokyo, Japan) operating at 200 kV. For the metallographic analysis, the samples were subjected to electrolytic etching. For the electrolytic etching process, a reaction cell containing concentrated HNO_3 as the liquid electrolyte was utilized. The cell consisted of two electrodes: an anode and a cathode. The sample, which was to be etched, was connected as the anode, while a stainless-steel cathode was employed for the etching process. To initiate the reaction, a voltage of 3 V was applied to the electrodes using an external power supply. Thin foils for transmission electron microscopy (TEM) were prepared by mechanically grinding the samples to 90 μm and then further thinned to perforation using a twinjet electrolytic polisher with a solution consisting of 10% $HClO_4$ in CH_3COOH at 25 V. The size of structural elements was measured by the random sectioning method using Image Expert Professional 3 software V3.7.5.0 (New Expert Systems, Ltd.; Moscow, Russia). X-ray diffraction (XRD) analysis was conducted using an Ultima IV diffractometer (Rigaku; Tokyo, Japan) at room temperature. Co Kα radiation at 40 kV and 30 mA was utilized. The XRD measurements involved scanning a 2θ range from 45° to 128° with a step size of 0.1° and a scanning speed of 1.5°/min. To minimize potential errors, the specimens for XRD analysis were mechanically ground and then electropolished prior to testing. Differential scanning calorimetry (DSC) was utilized to determine the temperature range of phase transformation. The measurements were conducted using a NETZCH DSC 404 F1 instrument under a protective argon atmosphere. The thermal stability of Cr-Ni-Ti steel after rotary swaging was studied by measuring the microhardness after annealing in the temperature range of 100–900 °C with a holding time of 1 h. For the high-cycle fatigue tests ($N = 10^7$ cycles), a repeated tension condition was applied using an INSTRON 8801 servohydraulic machine (Instron, Norwood, MA, USA)with a load capacity of 100 kN. The tests were carried out at a testing frequency of 40 Hz and a stress ratio of R = 0.1 using the samples shown in the Figure 2b.

3. Results

3.1. Metallographic Features of the Cr-Ni-Ti Steel after Quenching and Rotary Swaging

The microstructure of the Cr-Ni-Ti stainless steel in the initially quenched state and after RS was studied by light microscopy (Figure 3). Predominantly austenitic coarse-grained structures, with an average grain size of about 25 μm and with the presence of annealing twin boundaries and about 7.6% of the bcc-phase (retaining δ-ferrite), as confirmed by XRD (Figure 3a), were observed.

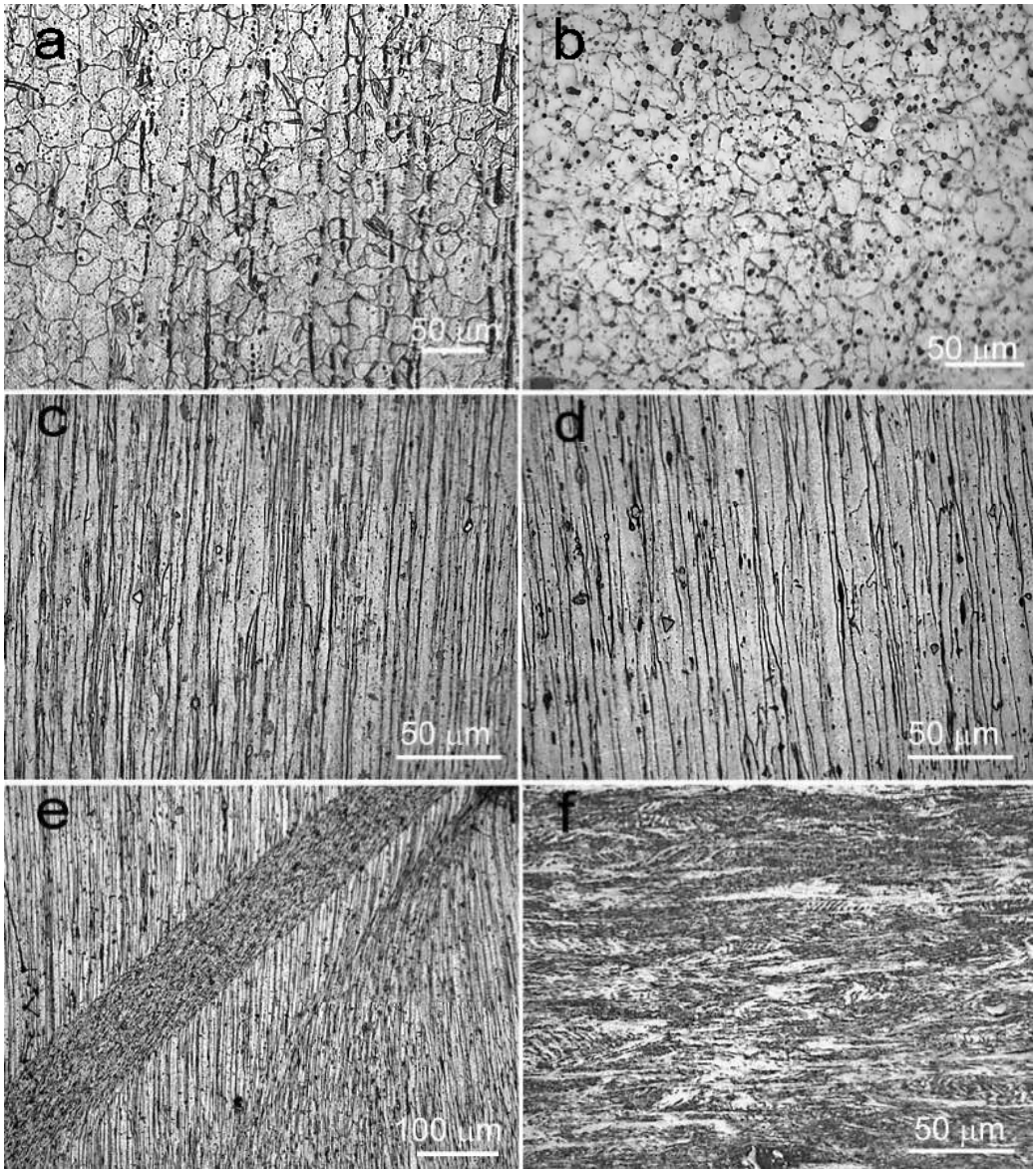

Figure 3. Light micrographs of Cr-Ni-Ti steel microstructure after quenching (**a**) and RS (μ = 10) (**b**–**f**) by regimes at: RS 450 °C (cross section) (**b**); RS 450 °C (**c**); RS 450 °C→200 °C (longitudinal section) (**d**); RS 450 °C→20 °C (longitudinal section) (**e**) and RS 450 °C→20 °C with subsequent annealing at 475 °C (**f**).

RS introduces significant changes in the structure of the steel (Figure 3c–e). After RS, according to the isothermal mode of deformation at a temperature of 450 °C with a total drawing (μ) equal to 10, the initial grain extended in the longitudinal direction was metallographically revealed up to 4.55 ± 0.4 μm in the cross section (Figure 3b). A similar structure with an average grain size in the cross section of 5.10 ± 0.34 μm corresponds to a stepwise regime with a temperature decrease RS 450 → 200 °C (μ = 10). The effect of more intense deformation resulted in shear bands visible in an optical microscope in samples after RS at a temperature of 450 °C, with a decrease in the deformation temperature to room temperature (RS 450 → 20 °C). In this case, the initial grain is stretched to 4.02 ± 0.24 μm in the cross section. At the same time, the internal structure of the grain is not detected even when examined by scanning electron microscopy (Figure 4). It should be noted that SEM shows significant structural changes in the RS-treated steel with a decreasing deformation temperature (RS 450 → 20 °C), which occurs after annealing at a temperature of 475 °C (Figure 4b).

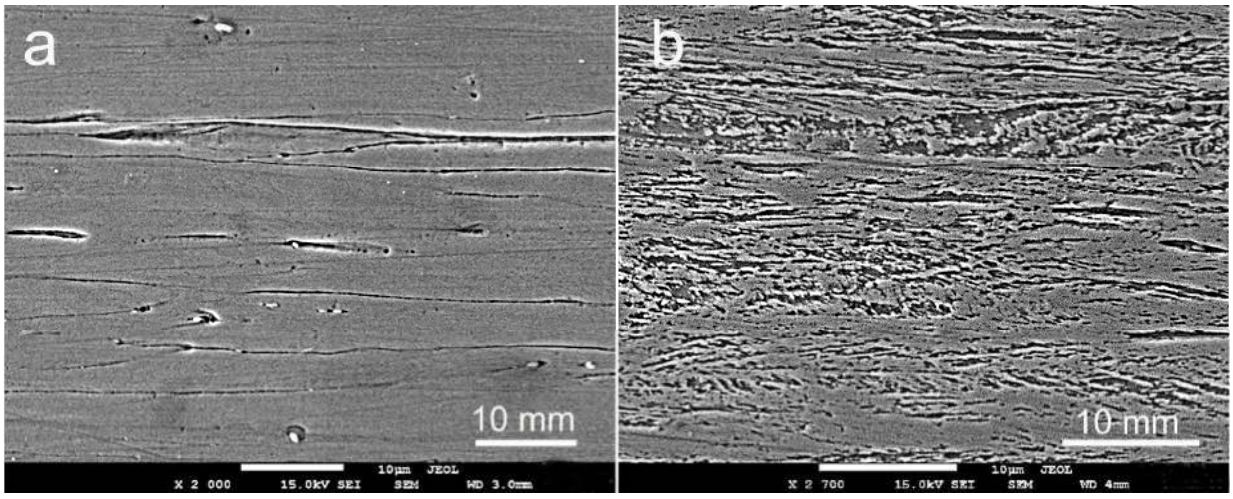

Figure 4. SEM analysis of microstructure of the Cr-Ni-Ti steel after RS by regimes: at RS 450 →20 °C (**a**) and at RS 450 →20 °C with subsequent annealing at 475 °C for 1 h (**b**).

3.2. X-ray Phase Analysis of the Cr-Ni–Ti Steel after Rotary Swaging and Subsequent Annealing

X-ray phase analysis revealed a predominantly austenitic steel structure for two regimes in the state after RS 450 °C, as well as for the regime with a decrease in the deformation temperature RS 450 → 200 °C (Figure 5, Table 2). The structure contains a bcc-phase ranging from 6% to 10%, which corresponds to the presence of retained δ-ferrite in the initial steel structure (Figure 5, Table 2). In the course of deformation according to the RS mode, with a stepwise decrease in temperature to room one RS 450 → 20 °C, a martensitic $\gamma \rightarrow \alpha'$ transformation occurs. It is confirmed by the presence of a 68% α-phase (~60% α-martensite) in the steel structure (Figure 5a, Table 2). After the annealing of the steel results in deformation, according to this mode, the amount of the α-phase in the steel structure increases up to 90% (Figure 5b, Table 2).

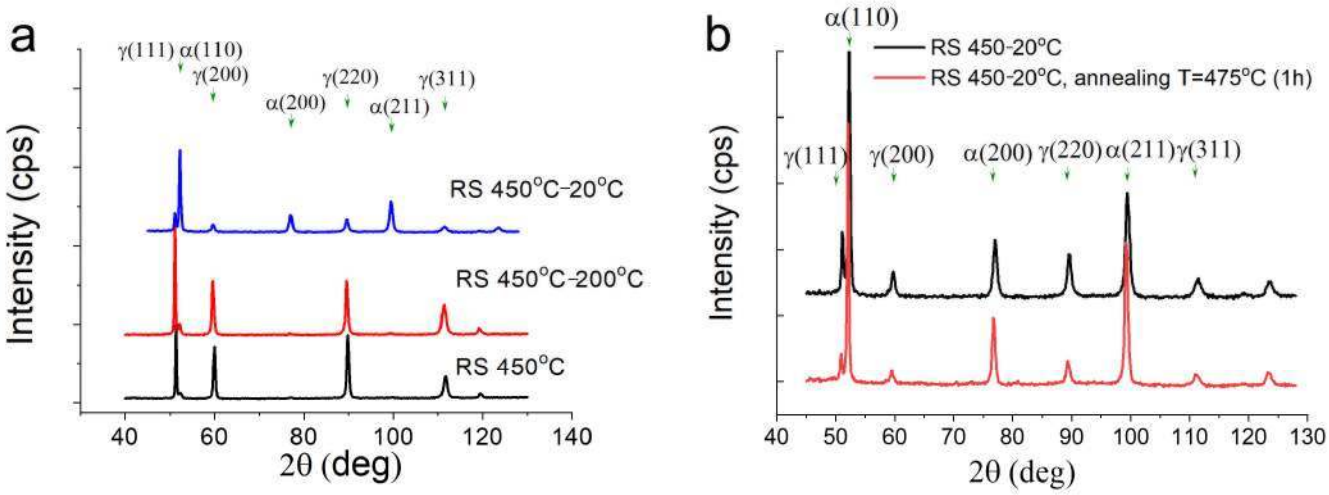

Figure 5. X-ray diffractions of the Cr - Ni-Ti steel samples produced by RS via different modes (**a**) and by RS 450 → 20 °C with annealing at 475 °C for 1 h (**b**).

Table 2. Fraction of γ and α—phase, crystallite size, and microstrain in the Cr-Ni-Ti steel after RS determined by X-ray line profile analysis.

Condition	Phase	Fraction, [vol.%]	a [Å]	Crystallite Size [Å]	ε, [%]
RS 450 °C, μ = 10	γ	94.0(14)	3.5900(3)	524(55)	0.200(9)
	α	6.0(7)	2.872(3)	1000(148)	0.61(4)
RS 450 → 200 °C, μ = 10	γ	90.0(13)	3.5971(3)	260(14)	0.184(17)
	α	10.0(19)	2.8795(12)	939(154)	0.40(3)
RS 450 → 20 °C, μ = 10	γ	32.0(5)	3.5903(10)	686(243)	0.325(12)
	α	68.0(9)	2.8718(3)	562(81)	0.270(9)
RS 450 → 20 °C, μ = 10, annealing at 475 °C	γ	10.0(9)	3.5972(10)	210(100)	0.20(12)
	α	90.0(8)	2.87512(11)	310(170)	0.20(12)

3.3. Transmission Electron Microscopy (TEM) Studies of Cr-Ni-Ti Steel after Rotary Swaging

The TEM analysis revealed that the steel samples after the isothermal regime RS 450 °C have an ultrafine-grained structure with shear bands ranging from 100 to 600 nm in thickness. These shear bands are intersected by thick dislocation walls and thin twin lamellae with a thickness of 18.2 ± 2 nm (Figure 6a,b). Numerous diffraction spots, besides those belonging to the <111> zone axis in SAED pattern taken from the area of Ø1400 nm in Figure 5a, suggest rather large misorientations evolved within the shear bands. With a decrease in the final deformation temperature to 200 °C, the thickness of the shear bands decreases (50–400 nm), the density of twins becomes higher, and the twins themselves become thinner (13.2 ± 1.8 nm) (Figure 6c,d).

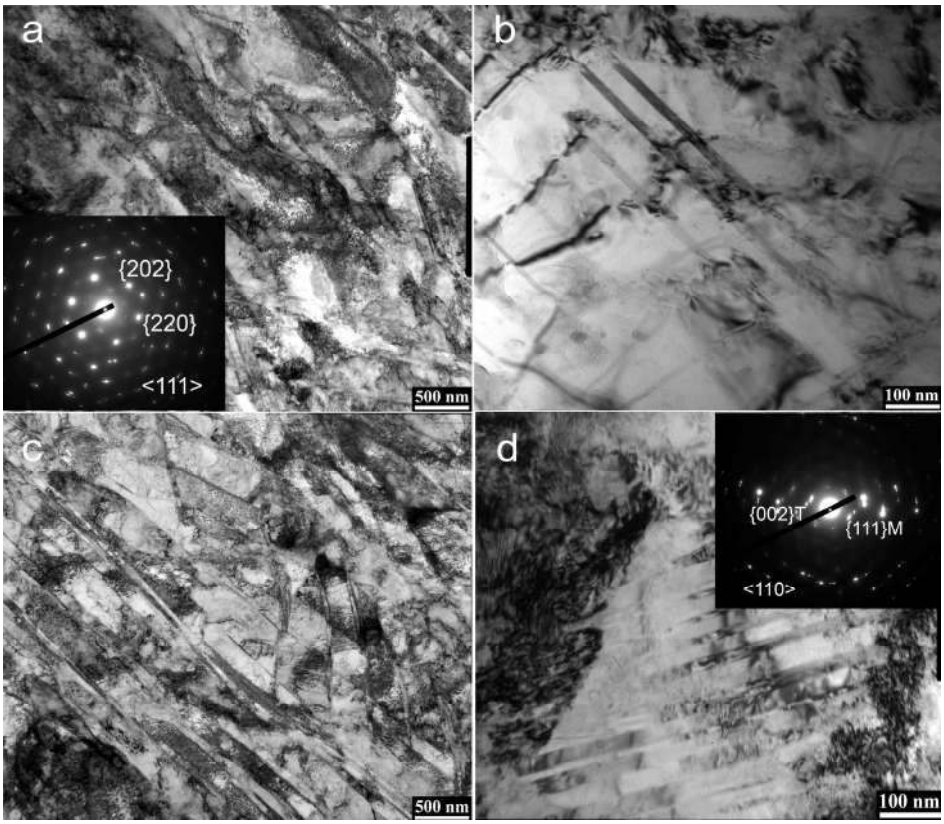

Figure 6. TEM micrographs and selected area electron diffraction (SAED) patterns for the samples of the Cr-Ni-Ti steel after RS by regime RS 450 °C (**a**,**b**) and RS 450 → 200 °C (**c**,**d**).

The average size of the structural elements of steel samples after RS, according to the regime with a stepwise decrease in temperature RS 450 → 20 °C, is 128 ± 6 nm. Martensite packets with a lamellar thickness ranging from 4 nm to 27 nm are observed (Figure 7a,b). The ring-like SAED pattern in Figure 6a is indicative of large misorientations in the developed microstructures.

Annealing at 475 °C, after rotary swaging by regime RS 450 → 20 °C (Figure 7c,d), does not increase the average size of structural elements with high-angle grain boundaries, as suggested by the ring-like SAED pattern taken from the area of Ø1400 nm in Figure 7c. Also, the diffraction pattern in the inset (Figure 7c) reveals multiple reflections from dispersed particles. On the electron diffraction pattern of the sample after rotary swaging, only reflections from the γ and α' phases can be identified. Figure 8a shows a ring electron diffraction pattern with marked reflections corresponding to the γ- and α'-phases (from the center to the edge): {111}γ (2.08Å); {200}γ (1.80Å); {200}α (1.43Å); {220}γ (1.27Å); {211}α (1.17Å), etc.)

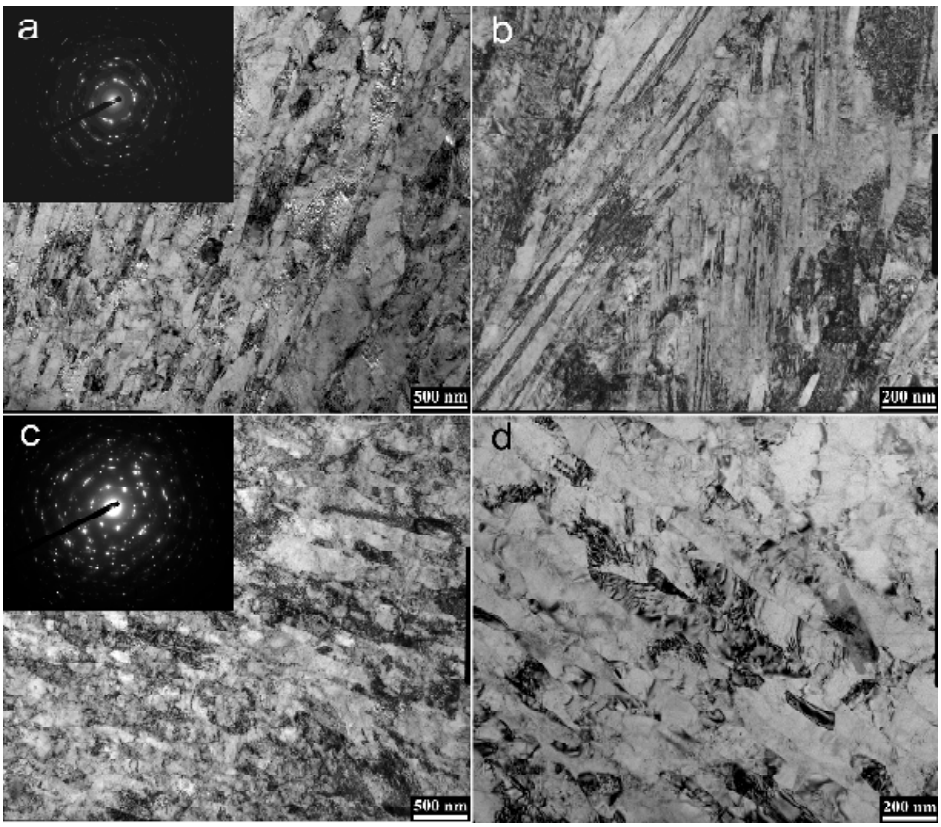

Figure 7. TEM micrographs and SAED (the area of Ø1400 nm) patterns for the samples of the Cr-Ni-Ti steel after RS by regime RS 450 → 20 °C (**a**,**b**) and RS 450 →20 °C with subsequent annealing (**c**,**d**).

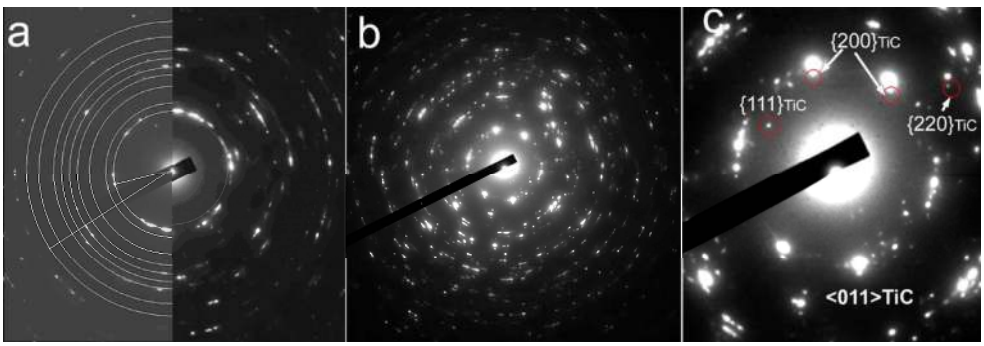

Figure 8. SAED (the area of Ø1400 nm) pattern from TEM images of the microstructure of Cr-Ni-Ti steel after RS by regime: at T_{RS} = 450 → 20 °C (**a**) and at T_{RS} = 450 → 20 °C with annealing (**b**,**c**).

Annealing at 475 °C leads to the formation of multiple additional reflections on the electron diffraction pattern that do not correspond to the austenitic and ferritic phases (Figure 8b). It is likely that these additional reflections could be the reflections from the particles of TiC. In the enlarged central part of the diffraction pattern, reflections corresponding to this type of precipitates are marked with red circles (Figure 8c).

3.4. Microhardness of the Cr-Ni-Ti Steel after Rotary Swaging and Subsequent Annealing

The thermal stability of the Cr-Ni-Ti steel after rotary swaging was studied by the determination of microhardness after annealing in the temperature range between 100 and 900 °C (Figure 9). In the context of this study, the investigation of microhardness as a function of annealing temperature reveals not only the level of steel strengthening depending on the processing conditions, but also the temperature of recrystallization initiation and the potential formation of strengthening particles. The microhardness of the Cr-Ni-Ti steel, after rotary swaging with stepwise deformation RS 450 → 20 °C, is significantly increased by annealing at 475 °C for 1 h.

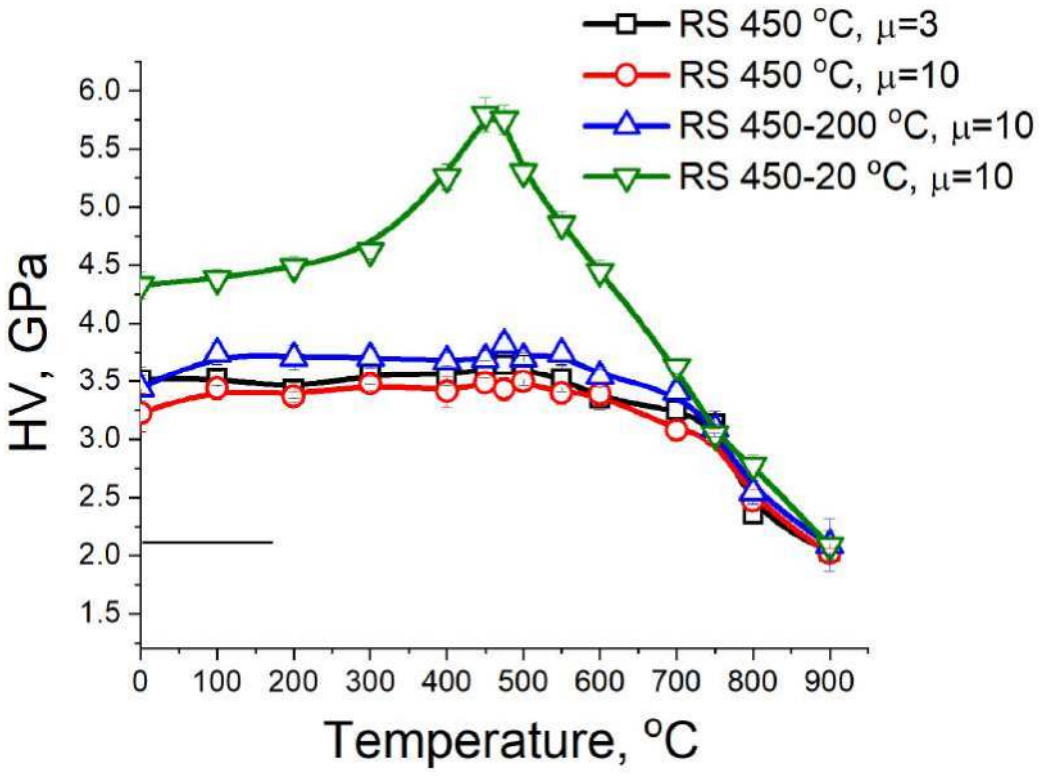

Figure 9. Microhardness of the Cr-Ni-Ti steel samples after RS and subsequent annealing.

This increase in microhardness of the steel, after rotary swaging with stepwise temperature reduction RS 450 → 20 °C, followed by annealing in the temperature range of 300–550 °C, is a result of the precipitation of nanoscale TiC carbides. The reflections from these carbides are represented in Figure 8c.

3.5. DSC Analysis

In this study, the process of particle precipitation in the temperature range of 300–550 °C was simulated using non-isothermal heating in differential scanning calorimetry (DSC) for a deformed steel sample, according to the RS 450 → 20 °C mode. DSC analysis allows the detection of particle precipitation (exothermic reactions) through peaks on the curves and the determination of the process characteristics, including the onset temperature of particle precipitation (365.4 °C), the temperature range of precipitation (365.4–526 °C), and the amount of heat released per gram of substance (H = 12.18 J/g) (Figure 10). DSC

confirmed the precipitation of carbides in the steel during annealing in the temperature range of 365.4–526 °C.

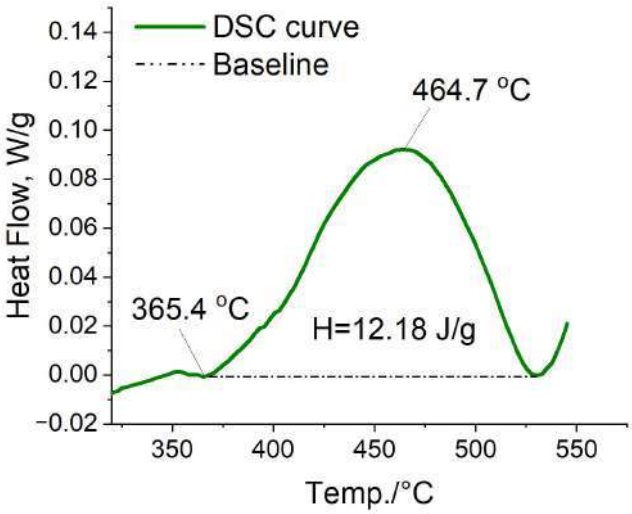

Figure 10. DSC analysis of the Cr-Ni-Ti steel produced by RS via step-wise mode with decreasing processing temperature 450 → 20 °C.

3.6. Mechanical Properties of the Cr-Ni-Ti Steel after Rotary Swaging

3.6.1. Tensile Tests

The results of uniaxial tension tests are presented in Table 3 and Figure 10. The steel samples in their initial state have a yield strength (σ_{YS}) of 313 MPa, an ultimate tensile strength (σ_{UTS}) of 601 MPa and an elongation (ε) of 50%. RS leads to an increase in σ_{UTS} within the range of 771–1304 MPa, σ_{YS} within the range of 683–1248 MPa, and a reduction in ε from 40% to 10.5% (Figure 11, Table 3). Thus, the investigation of the mechanical properties revealed that the RS of the Cr-Ni-Ti steel with μ = 10, when the deformation temperature is reduced from 450 °C to room temperature, increases σ_{UTS} by 1.5–2 times and σ_{YS} by 2.7–4 times (Figure 11, Table 3).

Table 3. Mechanical properties of Cr-Ni-Ti stainless steel after rotary swaging.

№	Condition	σ_{UTS} [MPa] [1]	σ_{YS} [MPa] [2]	ε [%] [3]
1.	RS 450 °C, μ = 3	771	683	40
2.	RS 450 °C, μ = 10	897	833	17
3.	RS 450 → 200 °C, μ = 10	1042	952	17
4.	RS 450 → 20 °C, μ = 10	1304	1248	10.5
5.	RS 450 → 20 °C, μ = 10, annealing at 475 °C	1939	1610	8
6.	Quenching, T_q = 1050 K (water cooling)	601	313	50

[1] σ_{UTS}—ultimate tensile strength; [2] σ_{YS}—yield strength; [3] ε—total elongation.

Annealing at 475 °C further enhances the strength properties with σ_{UTS} of 1939 MPa and σ_{YS} of 1610 MPa, along with a relatively small decrease in ductility. This results in an increase of σ_{UTS} by 3.2 times and σ_{YS} by 5 times compared to the initial state (Figure 10, Table 3). Significant increase in the strength of the Cr-Ni-Ti steel after annealing is achieved due to dispersion hardening through the formation of nanoscale TiC carbides in a highly defected martensitic structure. This strengthening mechanism contributes to the improved mechanical properties of the steel by hindering dislocation movement and promoting grain refinement.

It should be noted that the Cr-Ni-Ti steel achieved a high level of yield strength, ranging from 683 to 1610 MPa, after all the rotary swaging regimes. This is significant because the yield strength of austenitic stainless steels is typically low, which often limits

their range of applications. The substantial improvement in yield strength observed in this study enhances the potential uses of Cr-Ni-Ti steel in various industrial applications.

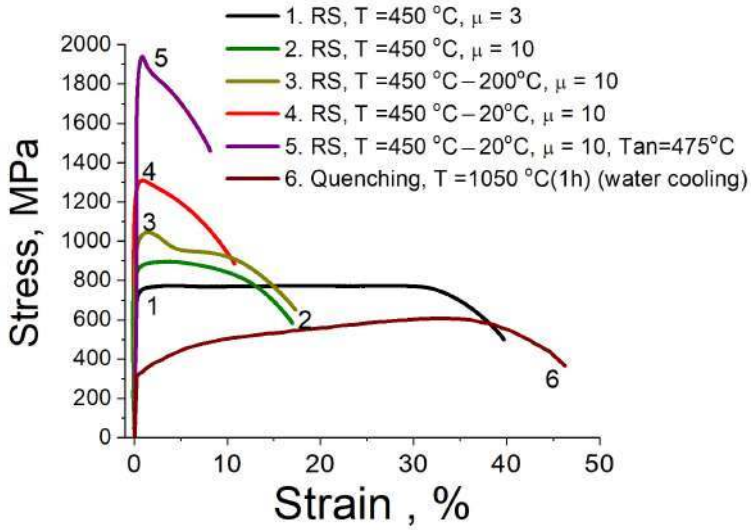

Figure 11. Tensile tests of Cr-Ni-Ti stainless steel after quenching and rotary swaging via different mode with decreasing processing temperature of 450 → 20 °C and subsequent annealing.

3.6.2. High-Cycle Fatigue Tests

Typically, an increase in yield strength is accompanied by an improvement in fatigue strength. Indeed, this study, conducted on Cr-Ni-Ti stainless steel after RS 450 → 20 °C, demonstrated a significant enhancement in the fatigue limit of the steel under cyclic loading conditions (up to 700 MPa compared to 425 MPa after quenching), as shown in Figure 12. This enhancement in fatigue strength indicates the beneficial effect of rotary swaging on improving the fatigue resistance and durability of the steel.

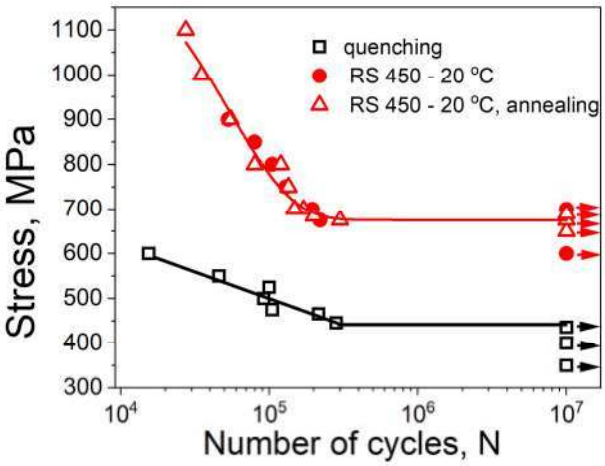

Figure 12. The Woehler (S-N) curves for cyclic deformation of Cr-Ni-Ti stainless steel before and after rotary swaging.

However, the observed dispersion strengthening in Cr-Ni-Ti stainless steel after the stepwise RS 450 → 20 °C and subsequent annealing (T = 475 °C) does not alter the fatigue limit of the steel obtained after deformation. It appears that the loss of ductility in the investigated steel after the processing methods may actually promote easier initiation and propagation of fatigue cracks. Despite this, the fatigue limit of the steel remains at the same level after annealing, as observed after RS 450 → 20 °C.

4. Discussion

It was found that the ultrafine-grained structure in the steel under study is formed by two mechanisms. The first one is associated with the fragmentation of the original grains due to the formation of deformation shear bands and deformation twins. The second one is associated with the development of the $\gamma \rightarrow \alpha'$ phase transformation through the shear mechanism of formation of deformation martensite. During deformation by the RS 450 °C regime (Figure 6a,b), deformation bands with a large accumulation of dislocations and the presence of deformation twins are formed. In the stepwise RS 450 → 200 °C regime, the shear bands become thinner, and twins begin to play a greater role in the formation of the spatial network of high-angle boundaries. Twins, along with dislocation walls and cut shear bands form a UFG structure. Moreover, in this regime, martensitic transformation can also play a role in the formation of new nanograins (Figure 5a). During deformation at RS 450 → 20 °C, martensitic transformation becomes the main mechanism ensuring structure refinement.

The main approach of this work was the choice of the optimal temperature regimes of RS, focusing on the possibility of the onset of martensitic transformation. Among of all the RS modes, only the mode with a stepwise decrease in the deformation temperature RS 450 → 20 °C leads to the formation of strain-induced martensite in a significant amount. In the other RS regimes, where the deformation was completed at temperatures of 200 °C or 450 °C, the formation of strain-induced martensite was either unlikely (at 200 °C) or excluded (at 450 °C) because the temperature of the final stage of deformation exceeded or was close to the onset of strain-induced martensite. Therefore, in these cases, the main phase is austenite. The strength of Cr-Ni-Ti steel in the austenitic state increased as the temperature of the end of RS decreased. Moreover, the dependence of the change in microhardness of the steel samples after isothermal RS 450 °C and after the regime with decreasing processing temperature RS 450 → 200 °C during annealing is the same, since the initial phase state (austenite) was the same.

During annealing of the steel samples after RS, with a decrease in temperature RS 450 → 20 °C, dispersion hardening of the main martensite phase occurs, together with the processes in the retained austenite. There are typical processes occurring in such steels at 475 °C. Namely, the formation of carbide ($Cr_{23}C_6$, or titanium carbide TiC), intermetallic formation ($TiNi_3$) processes causing 475-degree embrittlement (ordering and delamination in the Fe-Cr system, especially in the α phase). This can cause a noticeable peak in the temperature dependences of the microhardness and yield strength. The peak on the DSC curve at 465 °C indicates the development of at least some or even all of these processes. At the same time, it should be noted that deformation could shift the temperature intervals for the realization of certain processes.

The structure of the studied steel after deformation by RS 450 → 20 °C consists of austenite and martensite (Figure 4a,b). Despite the fact that the density of dislocations generated during deformation decreases to some extent upon heating, a noticeable strengthening of the steel is already observed. During the initial stage of martensite aging, it can be assumed that segregations or regions enriched with alloying element atoms are formed. These areas act as nuclei for the precipitating phase. The presence of segregations and precipitations usually leads to an increase in the etching ability of structural element boundaries, which can be observed in Figures 3f and 4b. It should be noted that studying the early stages of martensite aging by electron microscopy is challenging due to the high density of dislocations. However, during TEM analysis, reflections from TiC carbide were detected in the selected area electron diffraction patterns (Figure 8b,c).

This study revealed that the grain refinement during the rotary swaging process, as well as dispersion hardening through the precipitation of fine carbides during subsequent annealing, led to a significant increase in the strength properties of the metastable austenitic steel. It should be noted that the tensile curves for the samples after stepwise RS 450 → 20 °C mode with and without annealing (curves 4,5) are somewhat different from the others. Corresponding tension diagrams are characterized by a sharp abrupt transition

in the shape of a tooth from the elastic region to the plastic region. This behavior is typical for bcc materials, when the formation of impurity atmospheres (Cottrell, Suzuki, Snuka) on dislocations complicates the movement and increases the voltage necessary for the start of the operation of dislocation sources [42]. In addition, the resulting structure is an UFG with a large volume of grain boundary surfaces primarily responsible for dislocation glide. The increased density of dislocations and grain boundaries formed during the rotary swaging process leads to the accumulation of dislocations, hindering their further movement and thereby increasing the yield strength. Dispersion strengthening during annealing operates in a similar manner by impeding dislocation motion and promoting grain refinement. The combination of these mechanisms contributes to the overall improvement in the strength of the material.

Due to the fact that the initiation of fatigue cracks is also a result of dislocation sliding, such processing methods as RS should not only lead to a significant increase in strength but also a substantial improvement in fatigue limit. This was demonstrated on Cr-Ni-Ti stainless steel samples after the stepwise rotary swaging with temperature reduction RS 450 $\rightarrow$ 20 °C. However, annealing following this processing, which was accompanied by dispersion strengthening, did not increase the fatigue limit of Cr-Ni-Ti stainless steel obtained after deformation. It is possible that the loss of ductility in the investigated steel facilitates easier initiation and propagation of fatigue cracks. Up to a certain level of strengthening achieved after the stepwise deformation RS 450 $\rightarrow$ 20 °C, there is still some improvement in the fatigue limit. After significant strengthening due to dispersion hardening from subsequent annealing, there is no further improvement in fatigue strength due to the lack of ductility reserve. However, despite the absence of further improvement in fatigue strength, the fatigue limit of the steel remains at the same high level after annealing as observed after deformation.

The mechanical characteristics of samples obtained after rotary swaging show the prospects of using this method for processing stainless steels. In this work, stepwise rotary swaging followed by annealing at 475 °C resulted in an excellent combination of strength and ductility (σ_{UTS} = 1939 MPa and ε = 8.2%, respectively). A similar strength value (1855 MPa) was previously achieved only using high pressure torsion (Table 4). It is necessary to take into account that in the case of HPT, the ductility of steel is two times lower than that obtained in this study [5]. In addition, HPT is mostly a model processing method that makes it possible to study the structure formation of a material at very high degrees of deformation. In contrast, rotary swaging is an industrially applicable deformation method that makes it possible to obtain long-length workpieces of various diameters.

Table 4. Mechanical properties of different Cr-Ni-Ti stainless steels (HPT—high pressure torsion; ECAP—equal-channel angular pressing).

Steel	Condition	σ_{UTS} [Mpa]	σ_{YS} [Mpa]	ε [%]	Reference
Fe-17.3Cr-9.2Ni-0.7Ti	Quenching, T_q = 1323 K (water cooling)	601	313	50	Present study
	RS, T_{RS} = 450 $\rightarrow$ 20 °C, μ = 10, annealing at 475 °C	1939	1610	8.2	
0.08C–18Cr–10Ni–Ti	HPT	1855	-	~4	[11]
Fe-17.3Cr-9.2Ni-0.7Ti	ECAP, N = 4, ~25 °C	1228	1173	11	[5]
AISI 321L (Fe-0.08% C-17.9% Cr-10.6% Ni-0.5% Si-0.1% Ti)	ECAP, N = 4, T = 150 °C	1100	-	45	[40]
Fe-17.3Cr-9.2Ni-0.7Ti	ECAP, N = 6, T = 450 °C	1009	900	21	[43]
08C-18Cr-10Ni-Ti	ECAP, N = 8, T = 400 °C	1020	990	14	[44]
AISI 321	Cold rolling	1270	-	14.7	[45]
Fe-18.02Cr-9.77Ni-1.4Mn-0.59Ti-0.39Si-0.19Cu-0.1Mo-0.08C (wt.%)	Hot rolling (1100 °C, e = 0.8, 1 pass) + Hot rolling (600 °C, e = 0.7)	793 $\pm$ 34	677 $\pm$ 34	12 $\pm$ 6	[46]
0.12 C–18Cr–10Ni–Ti	ABC pressing + rolling	1133 $\pm$ 15	867 $\pm$ 11	32 $\pm$ 1.5	[47]
AISI-321	Radial-shear rolling	1073	-	21	[48]

The strength values obtained in an earlier study [11] on this steel, using the ECAP method at room temperature (σ_{UTS} = 1228 MPa, σ_{YS} = 1173 MPa), are significantly lower (Table 4) than those obtained in this work (Table 3). Increasing the ECAP temperature to 150 °C leads to a decrease in strength (σ_{UTS}) to 1100 MPa (which is 43% lower than the value obtained in this study) while increasing ductility (ε) to 45% [40]. An increase in the ECAP temperature to 450 °C in the study [41] leads to the formation of lower strength values and a twofold growth of ductility (σ_{UTS} = 1009 MPa, ε = 21%) compared to samples of the same steel after ECAP at room temperature [11]. In the study [44], at an ECAP temperature of 400 °C and a higher number of ECAP passes (N = 8), it was found that while the strength slightly increased compared to the deformation regime in [43], the ductility significantly decreased (ε = 14%). The level of strength achieved through ECAP in [40,43,44] is comparable to the strength obtained through traditional deformation methods such as cold rolling [45], pressing combined with rolling [47], and radial-shear rolling [48]. In contrast, hot rolling produces a state with noticeably lower strength [45]. Thus, it should be noted that the application of rotary swaging for processing Cr-Ni-Ti stainless steel, such as type 321, allows to produce the high-strength long-length workpieces comparable in strength to samples subjected to severe plastic deformation. This highlights the promising potential of rotary swaging in industrial applications.

5. Conclusions

The application of rotary swaging and subsequent heat treatment, in order to modify the structure and properties of metastable austenitic Cr-Ni-Ti stainless steel, has resulted in outstanding strength characteristics due to the refinement of the structure and occurrence of phase transformations. The following findings were obtained during the study:

1. The formation of an ultrafine-grained predominantly twinned structure with structural elements sized between 100–250 nm in Cr-Ni-Ti stainless steel was observed.
2. By reducing the temperature of the end of the step-wise rotary swaging to 200 °C, the density of deformation twins in the microstructure is increased, and their thickness is reduced. Further lowering the temperature to room one RS 450 →20 °C leads to a deformation-induced $\gamma \rightarrow \alpha'$ martensitic transformation, resulting in the formation of deformation martensite (up to 60%). This sequence of temperature reductions during RS allows for the manipulation of the microstructure and the phased transformations, ultimately leading to the desired properties in the steel.
3. The structure obtained through RS and subsequent annealing determined a high level of mechanical properties. The high-strength characteristics, exceeding the yield strength level in the initial state by 1.3–3.2 times, and the tensile strength by 2.1–5.1 times, are accompanied by the achievement of acceptable level of ductility.
4. The maximum level of strength (σ_{UTS} = 1939 MPa, σ_{YS} = 1610 MPa) was achieved in the samples after RS with temperature reduction from 450 to 20 °C, followed by annealing at 475 °C for 1 h. This significant improvement in strength is attributed to the precipitation hardening of the steel, which is achieved through the formation of nanoscale carbides in the high-defect structure of the martensite.
5. During the investigation of microhardness changes after one-hour annealing in the temperature range of 100–900 °C, a temperature range for carbide precipitation in the steel after RS 450 → 20 °C was established. This observation was confirmed using DSC.
6. The RS process with step-wise temperature reduction from 450 °C to 20 °C demonstrates a noticeable improvement in the fatigue strength of the steel under cyclic loading conditions, reaching up to 700 MPa. This significant enhancement in fatigue strength highlights the effectiveness of the RS process in improving the fatigue resistance and durability of the steel.
7. The precipitation hardening observed during the annealing of Cr-Ni-Ti stainless steel after rotary swaging with step-wise temperature reduction RS 450 → 20 °C does not affect the fatigue limit obtained after deformation.

Author Contributions: Conceptualization, O.R. and S.D.; methodology, N.M. and G.R.; software, G.R., V.T. and D.P.; validation, O.R. and N.M.; formal analysis, N.M. and O.R.; investigation, O.R., N.M., G.R., E.L., A.T., V.T. and D.P.; resources, A.T.; data curation, S.D., A.T. and E.L.; writing—original draft preparation, O.R.; writing—review and editing, G.R., S.D., V.Y. and N.M.; visualization, O.R. and E.L.; supervision, S.D. and V.Y.; project administration, O.R.; funding acquisition, S.D. All authors have read and agreed to the published version of the manuscript.

Funding: This research was carried out with a support of the Russian Federation state assignment of A. A. Baikov Institute of Metallurgy and Materials Science of the Russian Academy of Science (IMET RAS), Russia (Theme No. 075-01176-23-00).

Data Availability Statement: All data required to reproduce these experiments are presented in the article.

Acknowledgments: The scanning electron microscope measurements were done using research equipment of the Shared Facility Center at P.N. Lebedev Physical Institute of RAS "Center for the Study of High-Temperature Superconductors and Other Strongly Correlated Electronic Systems". The TEM analysis was carried out using equipment of the Joint Research Center «Technology and Materials» of Belgorod State National Research University.

Conflicts of Interest: The authors declare no conflict of interest.

References

1. Hajizadeh, K.; Kurzydlowski, K.J. On the possibility of fabricating fully austenitic sub-micron grained AISI 304 stainless steel via equal channel angular pressing. *Mater. Today Commun.* **2023**, *35*, 105641. [CrossRef]
2. Awang Sh'ri, D.N.; Zahari, Z.S.; Yamamoto, A. Effect of ECAP Die Angle on Mechanical Properties and Biocompatibility of SS316L. *Metals* **2021**, *11*, 1513. [CrossRef]
3. Dobatkin, S.V.; Skrotzki, W.; Rybalchenko, O.V.; Terent'ev, V.F.; Belyakov, A.N.; Prosvirnin, D.V.; Raab, G.I.; Zolotarev, E.V. Structural changes in metastable austenitic steel during equal channel angular pressing and subsequent cyclic deformation. *Mater. Sci. Eng. A* **2018**, *723*, 141–147. [CrossRef]
4. Hajizadeh, K.; Kurzydlowski, K.J. Microstructure Evolution and Mechanical Properties of AISI 316H Austenitic Stainless Steel Processed by Warm Multi-Pass ECAP. *Phys. Metals Metallogr.* **2021**, *122*, 931–938. [CrossRef]
5. Dobatkin, S.V.; Rybal'chenko, O.V.; Raab, G.I. Structure formation, phase transformations and properties in Cr–Ni austenitic steel after equal-channel angular pressing and heating. *Mater. Sci. Eng. A* **2007**, *463*, 41–45. [CrossRef]
6. Rybalchenko, O.V.; Dobatkin, S.V.; Kaputkina, L.M.; Raab, G.I.; Krasilnikov, N.A. Strength of ultra-grained corrosion-resistant steels after severe plastic deformation. *Mater. Sci. Eng. A* **2004**, *387–389*, 244–248. [CrossRef]
7. De Vincentis, N.S.; Kliauga, A.; Ferrante, M.; Avalos, M.; Brokmeier, H.-G.; Bolmaro, R.E. Evaluation of microstructure anisotropy on room and medium temperature ECAP deformed F138 steel. *Mater. Charact.* **2013**, *107*, 98–111. [CrossRef]
8. Wang, H.; Shuro, I.; Umemoto, M.; Kuo, H.-H.; Todaka, Y. Annealing behavior of nano-crystalline austenitic SUS316L produced by HPT. *Mater. Sci. Eng. A* **2012**, *556*, 906–910. [CrossRef]
9. Abramova, M.M.; Enikeev, N.A.; Valiev, R.Z.; Etienne, A.; Radiguet, B.; Ivanisenko, Y.; Sauvage, X. Grain boundary segregation induced strengthening of an ultrafine-grained austenitic stainless steel. *Mater. Lett.* **2014**, *136*, 349–352. [CrossRef]
10. Shuro, I.; Kuo, H.H.; Sasaki, T.; Hono, K.; Todaka, Y.; Umemoto, M. G-phase precipitation in austenitic stainless steel deformed by high pressure torsion. *Mater. Sci. Eng. A* **2012**, *552*, 194–198. [CrossRef]
11. Dobatkin, S.V.; Rybalchenko, O.V.; Enikeev, N.A.; Tokar, A.A.; Abramova, M.M. Formation of fully austenitic ultrafine-grained high strength state in metastable Cr–Ni–Ti stainless steel by severe plastic deformation. *Mater. Lett.* **2016**, *166*, 276–279. [CrossRef]
12. Dong, F.Y.; Zhang, P.; Pang, J.C.; Ren, Y.B.; Yang, K.; Zhang, Z.F. Strength, damage and fracture behaviors of high-nitrogen austenitic stainless steel processed by high-pressure torsion. *Scr. Mater.* **2015**, *96*, 5–8. [CrossRef]
13. Mine, Y.; Koga, K.; Takashima, K.; Horita, Z. Mechanical characterisation of microstructural evolution in 304 stainless steel subjected to high-pressure torsion with and without hydrogen pre-charging. *Mater. Sci. Eng. A* **2016**, *661*, 87–95. [CrossRef]
14. Tirekar, S.; Jafarian, H.R.; Eivani, A.R. Towards engineering of mechanical properties through stabilization of austenite in ultrafine grained martensite–austenite dual phase steel processed by accumulative roll bonding. *Mater. Sci. Eng. A* **2017**, *684*, 120–126. [CrossRef]
15. Jafarian, H.R.; Tarazkouhi, M.F. Significant enhancement of tensile properties through combination of severe plastic deformation and reverse transformation in an ultrafine/nano grain lath martensitic steel. *Mater. Sci. Eng. A* **2017**, *686*, 113–120. [CrossRef]
16. Jafarian, H.R.; Mousavi, S.H.; Anijdan, A.R.; Eivani, N.; Park, A. Comprehensive study of microstructure development and its corresponding tensile properties in nano/ultrafine-grained metastable austenitic steel during accumulative roll bonding (ARB). *Mater. Sci. Eng. A* **2017**, *703*, 196–204. [CrossRef]
17. Nakao, Y.; Miura, H. Nano-grain evolution in austenitic stainless steel during multi-directional forging. *Mater. Sci. Eng. A* **2011**, *528*, 1310–1317. [CrossRef]

18. Sun, G.S.; Du, L.X.; Hu, J.; Xie, H.; Misra, R.D.K. Low temperature superplastic-like deformation and fracture behavior of nano/ultrafine-grained metastable austenitic stainless steel. *Mater. Des.* **2017**, *117*, 223–231. [CrossRef]
19. Dolzhenko, P.; Tikhonova, M.; Odnobokova, M.; Kaibyshev, R.; Belyakov, A. Ultrafine-Grained Stainless Steels after Severe Plastic Deformation. *Metals* **2023**, *13*, 674. [CrossRef]
20. Sun, J.; Wang, X.; Li, J.; Shu, D.; Wang, S.; Peng, P.; Mao, Q.; Liu, T.; Lu, X.; Li, Y.; et al. Enhanced mechanical properties of ultrafine-lamella 304L stainless steel processed by multidirectional hot forging. *Vacuum* **2021**, *187*, 110116. [CrossRef]
21. Xu, D.M.; Li, G.Q.; Wan, X.L.; Xiong, R.L.; Xu, G.; Wu, K.M.; Somani, M.C.; Misra, R.D.K. Deformation behavior of high yield strength—High ductility ultrafine-grained 316LN austenitic stainless steel. *Mater. Sci. Eng. A* **2017**, *688*, 407–415. [CrossRef]
22. Järvenpää, A.; Jaskari, M.; Man, J.; Pentti Karjalainen, L. Austenite stability in reversion-treated structures of a 301LN steel under tensile loading. *Mater. Character.* **2017**, *127*, 12–26. [CrossRef]
23. Sun, G.S.; Du, L.X.; Hu, J.; Misra, R.D.K. Microstructural evolution and recrystallization behavior of cold rolled austenitic stainless steel with dual phase microstructure during isothermal annealing. *Mater. Sci. Eng. A* **2018**, *709*, 254–264. [CrossRef]
24. Roytburd, A.L. The present state of the theory of martensitic transformations. In *Imperfections in Crystalline Structure and Martensitic Transformations*; Osip, Y.A., Entin, R.I., Eds.; Nauka-Publishing House: Moscow, Russia, 1972; pp. 7–33. (In Russian)
25. Naydenkin, E.V.; Mishin, I.P.; Zabudchenko, O.V.; Lykova, O.N.; Manisheva, A.I. Structural-phase state and mechanical properties of β titanium alloy produced by rotary swaging with subsequent aging. *J. Alloys Compd.* **2023**, *935*, 167973. [CrossRef]
26. Yuan, L.; Wang, W.; Yang, M.; Li, Y.; Zhang, H.; Zhang, H.; Zhang, W. Microstructure and Texture of Thin-Walled Ti-6Al-4V Alloy Seamless Tubing Manufactured by Cold-Rotary Swaging. *JOM* **2021**, *73*, 1786–1794. [CrossRef]
27. Charni, D.; Ortmann-Ishkina, S.; Herrmann, M.; Schenck, C.; Epp, J. Mechanical properties of rotary swaged steel components. *Forsch Ingenieurwes* **2021**, *85*, 723–732. [CrossRef]
28. Liu, Y.; Liu, J.; Herrmann, M.; Schenck, C.; Kuhfuss, B. Material Flow in Infeed Rotary Swaging of Tubes. *Materials* **2021**, *14*, 58. [CrossRef]
29. Kocich, R.; Kunčická, L.; Benč, M. Development of microstructure and properties within oxide dispersion strengthened steel directly consolidated by hot rotary swaging. *Mater. Lett.* **2023**, *353*, 135276. [CrossRef]
30. Martynenko, N.; Rybalchenko, O.; Bodyakova, A.; Prosvirnin, D.; Rybalchenko, G.; Morozov, M.; Yusupov, V.; Dobatkin, S. Effect of Rotary Swaging on the Structure, Mechanical Characteristics and Aging Behavior of Cu-0.5%Cr-0.08%Zr Alloy. *Materials* **2023**, *16*, 105. [CrossRef]
31. Feng, W.; Wang, Z.; Sun, Q.; He, Y.; Sun, Y. Enhancing strength and electrical conductivity of Cu–Cr composite wire by two-stage rotary swaging and aging treatments. *Compos. B Eng.* **2022**, *231*, 109567. [CrossRef]
32. Fu, Z.; Gao, B.; Li, X.; Li, C.; Pan, H.; Niu, H.; Zhu, Y.; Zhou, H.; Zhu, X.; Wu, H.; et al. Improved strength-ductility combination of pure Zr by multi-scale heterostructured effects via rotary swaging and annealing. *Mater. Sci. Eng. A* **2023**, *864*, 144584. [CrossRef]
33. Singh, G.; Raj, R.; Vishnu Narayanan, K.I.; Arora, U.K.; Jayaganthan, R. The effect of die design on residual stresses of Zr-4 alloy processed by swaging. *Procedia Struct. Integr.* **2023**, *46*, 149–154. [CrossRef]
34. Martynenko, N.; Anisimova, N.; Rybalchenko, G.; Rybalchenko, O.; Serebryany, V.; Zheleznyi, M.; Shinkareva, M.; Gorbenko, A.; Temralieva, D.; Lukyanova, E.; et al. Effect of Rotary Swaging on Mechanical and Operational Properties of Zn–1%Mg and Zn–1%Mg–0.1%Ca Alloys. *Metals* **2023**, *13*, 1386. [CrossRef]
35. Feng, W.; Wang, Z.; Sun, Q.; He, Y.; Sun, Y. Effect of thermomechanical processing via rotary swaging on grain boundary character distribution and intergranular corrosion in 304 austenitic stainless steel. *J. Mater. Res. Technol.* **2022**, *19*, 2470–2482. [CrossRef]
36. Panov, D.; Kudryavtsev, E.; Naumov, S.; Klimenko, D.; Chernichenko, R.; Mirontsov, V.; Stepanov, N.; Zherebtsov, S.; Salishchev, G.; Pertcev, A. Gradient Microstructure and Texture Formation in a Metastable Austenitic Stainless Steel during Cold Rotary Swaging. *Materials* **2023**, *16*, 1706. [CrossRef] [PubMed]
37. Scheil, E. Uber die Umwandlung des Austenits in Martensit in Eisen-nickellegierungen unter Belastung. *Z. Anorg. Chem.* **1932**, *207*, 21. [CrossRef]
38. Umemoto, M.; Owen, W.S. Effects of austenitizing temperature and austenite grain size on the formation of athermal martensite in iron–nickel and iron–nickel–carbon alloys. *Metall. Trans.* **1974**, *5*, 2041–2046. [CrossRef]
39. Glezer, A.M.; Pankova, M.N. Martensitic transformation in microcrystalline melt-quenched Fe–Ni alloys. *J. Phys.* **1995**, *IV*, 5299–5303. [CrossRef]
40. Lobodyuk, V.A. Size effect upon martensitic transformations. *Phys. Met. Metallogr.* **2005**, *99*, 143–153.
41. Kopylov, V.I.; Nokhrin, A.V.; Kozlova, N.A.; Chegurov, M.K.; Gryaznov, M.Y.; Shotin, S.V.; Melekhin, N.V.; Tabachkova, N.Y.; Smetanina, K.E.; Chuvil'deev, V.N. Effect of σ-Phase on the Strength, Stress Relaxation Behavior, and Corrosion Resistance of an Ultrafine-Grained Austenitic Steel AISI 321. *Metals* **2023**, *13*, 45. [CrossRef]
42. Krawczynska, A.T.; Lewandowska, M.; Pippan, R.; Kurzydlowski, K.J. The effect of high pressure torsion on structural refinement and mechanical properties of an austenitic stainless steel. *J Nanosci Nanotechnol.* **2013**, *13*, 3246–3249. [CrossRef] [PubMed]
43. Rybalchenko, O.V.; Anisimova, N.Y.; Kiselevsky, M.V.; Belyakov, A.N.; Tokar, A.A.; Terent'ev, V.F.; Prosvirnin, D.V.; Rybalchenko, G.V.; Raab, G.I.; Dobatkin, S.V. The influence of ultrafine-grained structure on the mechanical properties and biocompatibility of austenitic stainless steels. *J. Biomed. Mater. Res.* **2020**, *108*, 1460–1468. [CrossRef] [PubMed]
44. Shamardin, V.K.; Abramova, M.M.; Bulanova, T.M.; Karsakov, A.A.; Fedoseev, A.E.; Obukhov, A.V.; Valiev, R.Z.; Alexandrov, I.V.; Raab, G.I.; Enikeev, N.A. Stability of the structure and properties of an ultrafine-grained Cr-Ni steel irradiated with neutrons in nuclear reactor core conditions. *Mater. Sci. Eng. A* **2018**, *712*, 365–372. [CrossRef]

45. Rezaei, H.A.; Shaban Ghazani, M.; Eghbali, B. Effect of post deformation annealing on the microstructure and mechanical properties of cold rolled AISI 321 austenitic stainless steel. *Mater. Sci. Eng. A* **2018**, *736*, 364–374. [CrossRef]
46. Litovchenko, I.; Akkuzin, S.; Polekhina, N.; Almaeva, K.; Moskvichev, E. Structural transformations and mechanical properties of metastable austenitic steel under high temperature thermomechanical treatment. *Metals* **2021**, *11*, 645. [CrossRef]
47. Shamarin, N.; Filippov, A.; Tarasov, S.; Podgornykh, O.; Utyaganova, V. The effect of the structural state of AISI 321 stainless steel on surface quality during turning. *Met. Work. Mater. Sci.* **2020**, *22*, 102–113. (In Russian) [CrossRef]
48. Nayzabekov, A.; Lezhnev, S.; Maksimkin, O.; Tsai, K.; Panin, E.; Arbuz, A. Microstructure and mechanical properties of austenitic stainless steel AISI-321 after radial shear rolling. *J. Chem. Technol. Metall.* **2018**, *53*, 606–611.